Vacuum 122 (2015) 179–186

Contents lists available at ScienceDirect

Vacuum

journal homepage: www.elsevier.com/locate/vacuum

Structural, mechanical, and sand erosion properties of TiN/Zr/ZrN multilayer coatings

Songsheng Lin [a, b, c, *], Kesong Zhou [a, b], Mingjiang Dai [b, c], Enhui Lan [c], Qian Shi [b, c], Fang Hu [b, c], Tongchun Kuang [a], Chunqiang Zhuang [d]

[a] School of Materials Science and Engineering, South China University of Technology, Guangzhou 510640, PR China
[b] National Engineering Laboratory for Modern Materials Surface Engineering Technology, Guangzhou 510650, PR China
[c] Department of New Materials, Guangzhou Research Institute of Non-ferrous Metals, Guangzhou 510650, PR China
[d] Beijing Key Lab of Microstructure and Properties of Advanced Materials, Beijing University of Technology, Beijing 100124, PR China

ARTICLE INFO

Article history:
Received 27 March 2015
Received in revised form
18 September 2015
Accepted 21 September 2015
Available online 25 September 2015

Keywords:
Multilayer coating
Mechanical properties
Erosion behavior
Failure mechanism

ABSTRACT

TiN/Zr/ZrN multilayer architectures with different period and number of cycles are designed and deposited on TC_{11} titanium alloys by vacuum cathodic arc ion plating method. Their mechanical, adhesive, and erosive properties are investigated. For the designed architectures with specific thickness, their hardness and critical load depended on the period of coatings, but are not sensitive to the number of cycles. The erosion wear resistance of TC_{11} substrate can be effectively improved by increasing the period of coating up to 24. The failure mechanism of bare TC_{11} titanium alloys are dominated by plastic deformation via cutting and plowing, while chipping and delamination probably dominate the failure mechanism of coated samples. Crack deflection and crack branching are also observed in eroded samples.

1. Introduction

Abrasion is one of the most intractable problems in industrial process. Statistics data show that about 80% component failures are caused by abrasion, indicating it has been one fatal factor in industrial applications [1]. Among different kinds of abrasion, sand particle erosion (SPE) is frequently observed in various fields such as aerospace, energy, machine, metallurgy, and building materials [2]. Extensive investigations have been carried out to reduce the erosion loss caused by SPE and to improve the service life of components. Surface treatment by anti-erosion coatings is considered as an effective method to protect materials from being eroded [3–7].

At an early stage, monolithic coatings with high hardness were frequently used as anti-erosion materials [8–12]. However, such kinds of monolithic coatings could be easily damaged due to brittle fracture under the condition of complex stress field generated by the impact of solid particle. Straight cracks were frequently observed in such single coatings [13,14]. Afterwards, multilayer coatings were proposed, which are composed of alternative soft and hard layers. Soft layers, taken as ductile materials, are adapted to absorb and balance external stress, and hard layers are served as the role of wear resistance.

The choice of materials constituent and the design of period and the number of cycle are key factors in determining erosion properties of designed architectures. Borawski et al. reported their synthesized multilayer Ti/TiN films and found that multilayer films with eight periodic cycles (TiN:Ti = 19:1) had better erosion performance [15,16]. In contrast, another multilayer system, i.e. TiN/CrN and pure Ti, shows very poor erosion resistance [17]. Besides, Rutherford et al. found that coatings with a harder and thicker top layer were effective to resist erosion caused by small particles, while Koehler et al. observed that multilayer systems with thinner top layers corresponded to better erosion resistance [18,19]. These previous results indicate that erosion performances of multilayer systems could be greatly changed due to specific architectures and constituent materials.

Except for architectures, the impact angle and velocity of erodent particles are also important parameters in sand particle erosion. Diverse impact angles have different effects on the erosion performance of coating systems. For example, celotta et al. performed an erosion test on Si_3N_4 ceramic materials using an impact

* Corresponding author. School of Materials Science and Engineering, South China University of Technology, Guangzhou 510640, PR China.
E-mail address: lss7698@126.com (S. Lin).

http://dx.doi.org/10.1016/j.vacuum.2015.09.026
0042-207X/

angle of 90° and 30° under the same impact velocity of 105 m/s [20]. The erosion rate is 30.2 mm^3/kg at 90° impact angle, and increases up to 40.1 mm^3/kg at 30° impact angle. This indicates the important effect of the impact angle on erosion properties. For CrN/NbN superlattice coatings, Purandare et al. report that the volume loss increased as the impact angle varied from 20 to 90° [21]. All these results reveal that the impact angle also greatly affects the erosion resistance of multilayer systems.

In this work, a new TiN/Zr/ZrN architecture with different period and number of cycles was designed as erosion resistant coatings. Here Zr is selected as constituent materials based on their low costs and wide industrial applications. Moreover, TiN and ZrN have high hardness and are often used as protective coatings for wear resistance. The influence of the number of cycles and the impact angle was investigated. The erosion mechanism of the new architectures was discussed under the typical impact angles of 30° and 90°.

2. Experimental

In this work, TiN/Zr/ZrN coatings with a similar film thickness were designed into 3, 12, and 24 cycle period, in which the ratio of Ti/TiN and Zr/ZrN were set as 1:1. The Ti was used as a buffer layer. After experimental optimization of the cycle period of multilayer coatings, the number of the cycle period was further increased up to 48 and 96. TC_{11} (Ti-6Al-3.5Mo-1.8Zr) titanium alloys with a size of Φ 50 mm × 8 mm were used as substrates. They were polished until the surface roughness (R_a) is lower than 0.4 μm. Then these polished substrates were ultrasonically cleaned by 5% metal cleaning agent, deionized water and dehydration in sequence. TiN/Zr/ZrN multilayer coatings were prepared by auto-control multi-arc ion plating equipment (AS700DTX). Twelve circular targets were equipped inside of the vacuum chamber, in which 8 targets were used for titanium (99.9%) and 4 targets for zirconium (99.9%). A mixture of high purity Ar and N_2 gases (99.999%) was introduced into the chamber during the deposition process. TiN/Zr/ZrN multilayer coatings were obtained by tuning gas flow and by alternately launching titanium and zirconium targets. Prior to deposition, substrates were cleaned by plasma with a high bias voltage of −1000 V for 30 min. The deposition temperature was set in the range of 300–350 °C, and the working pressure was 0.5–1.0 Pa. The current applied to the targets was varied from 70 A to 100 A. A negative bias voltage of 100 V–150 V was used during the deposition process.

Scanning Electron Microscopy (Nova Nano SEM 430) was employed to examine the surface and cross-section morphologies of multilayer coatings. The structure analysis was carried out by a Philips X'pert MPD diffractometer with Cu Ka radiation. The Vickers micro-hardness was measured by MD-5 hardness tester using a load of 25 g for 15 s. The hardness test was performed on three different positions of the film surfaces for each sample, and their averaged value was used. The adhesion strength was tested by a HH-3000 scratch instrument. A diamond tip was used to scratch the coating surface with a loading speed of 100 N/min, a horizontal velocity of 5 mm/min, and a maximum load of 100 N. The erosion test was conducted by AS600 sandblast tester (ASTM standard G76-05), the corresponding setup is schematically shown in Fig. 1.

During the deposition, the residual stress was generated in the multilayer films. The residual stress was mainly composed of the growth stress and the thermal stress. The growth stress was formed during the growth of the multilayer films, and the thermal stress was created from the difference of the thermal expansion between films and substrate. Both of them have strong effect on substrates, which further result in the bending of substrates. Based on substrates bending effects, the curvature radius of substrates before and after deposition process can be obtained by using wafer curvature techniques. Then the residual stress inside of multilayer films can be deduced by stress gauge (FST-150) according to the classical Stoney equation:

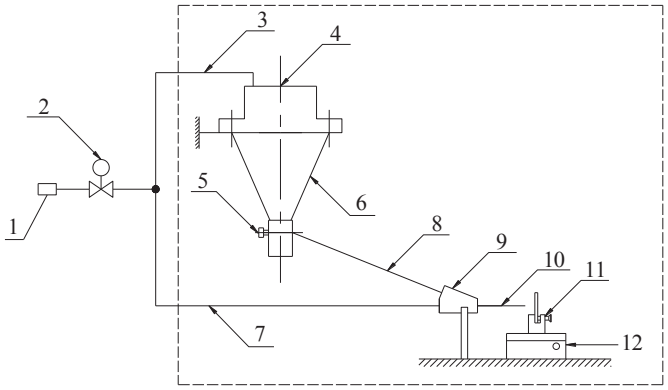

Fig. 1. Schematic diagram of the erosion device.

$$\sigma = \frac{E_s t_s^2}{6(1-\nu_s)\left(\frac{1}{R}-\frac{1}{R_0}\right)t_f}, \quad (1)$$

in which σ is the residual stress. E_s and ν_s is the Yong's modulus and the Passion ratio of substrate, respectively. t_s and t_f is the thickness of substrate and film, respectively. R_0 and R is the curvature radius of substrate before and after deposition. The elastic modulus of the TC_{11} alloy substrate (Ti-6Al-3.5Mo-1.8Zr) is 123 GPa, its passion ratio is 0.33. The size of the substrate is 17 mm × 60 mm × 1 mm. The surface of the substrate was treated by mechanical polishing. Meanwhile, the polished silicon crystal with the 100 orientation was also used as the substrate, with a size of 17 mm × 60 mm × 0.5 mm. Its elastic modulus and passion ratio is 130 GPa and 0.278, respectively. The curvature radius of these substrates was measured to evaluate the residual stress.

Alumina (Al_2O_3) powders with an average size of 55 μm were used as erodent particles (see Fig. 2). For each test, an impact velocity of 30 ± 2 m/s and an average particle feed rate of 2 ± 0.5 g/min were employed. Two representative impact angles, i.e. 30 ± 2°

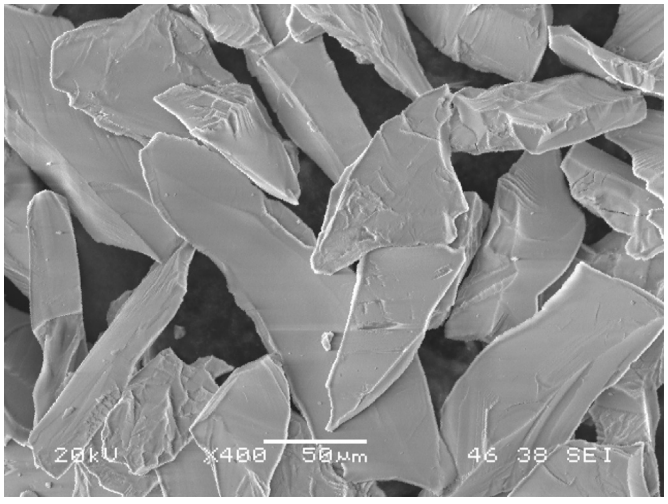

Fig. 2. Surface morphology of erodent particles.

and 90 ± 2°, were chosen. The 30° impact angle represents the glancing incidence and the 90° impact angle corresponds to normal impact. The morphology of erosion area was measured by BMT Expert 3D surface profiler. Elemental distribution was investigated by PHI-700 Scanning Auger Electron Spectrometer (AES), in which Ar^+ was applied to sputter the sample with energy of 5 kV and a sputtering rate of 4 nm/min.

3. Results and discussion

3.1. Multilayer coatings with different periods

Fig. 3 shows the cross-sections of TiN/Zr/ZrN multilayer coatings with 3, 12 and 24 cycle periods. The dark layer is TiN and the light one is Zr/ZrN. For coatings with 3, 12 and 24 periods, the total film thickness of these coatings is similar. The thickness is ~8 μm, which can be seen clearly from Fig. 3. The thickness of individual TiN/Zr/ZrN cycle period for coatings with 3, 12 and 24 periods is about 2.0 μm, 0.6 μm and 0.3 μm, respectively.

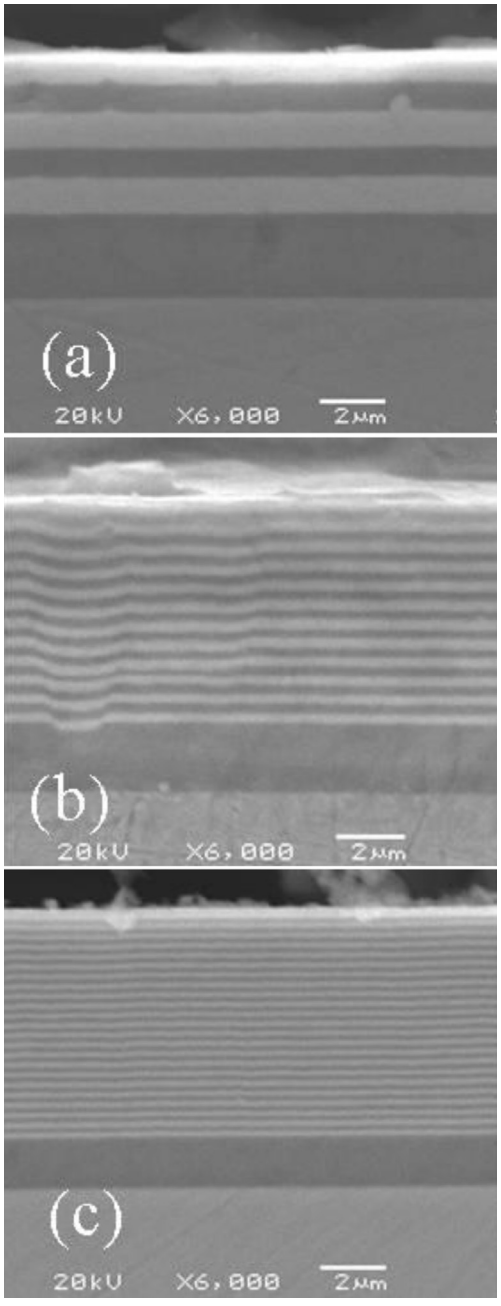

Fig. 3. Sectional morphologies with different modulated periods of TiN/Zr/ZrN multilayer coatings (a) 3 period, (b) 12 period, (c) 24 period.

The basic properties of the multilayer coatings are summarized in Table 1. TiN/Zr/ZrN coatings with the cycle period of 3, 12 and 24 have a hardness value of 25.83 GPa, 29.58 GPa, and 33.54 GPa, respectively. The thickness of one TiN/Zr/ZrN layer for 3 period is ~2.0 μm, in which the outermost ZrN layer is ~1.0 μm. The hardness for TiN/Zr/ZrN multilayer coatings (25.83 GPa) with 3 periods is very similar with that of ZrN coatings (25.73 GPa). For the coatings with 12 and 24 periods, the refined columnar structure and increased interface were obtained. As a result, the hardness of coatings increased with being increased cycle period. The adhesive test shows that corresponding critical load is 42 N, 50 N and 70 N for the sample with the period of 3, 12 and 24, respectively. These results reveal that mechanical properties of coatings with the same film thickness can be improved by increasing their number of cycle period.

The erosion test was carried with an attack angle of 30° and 90°, respectively. The results show that the coatings start to be damaged with the sand weight of ~19 g for the sample with 3 periods, ~21.7 g for the sample with 12 periods, and ~23.8 g for the sample with 24 periods at the impact angle of 30°. The coating with 24 cycle period has the best erosion properties. Multilayer coatings with the same film thickness show that their mechanical properties including hardness, adhesion and erosion resistance can be improved with increasing cycle period. Based on this consideration, coatings with 24 cycle period but different film thickness were further analyzed in the following sections, in which the TiN/Zr/ZrN individual layer has the same thickness of ~300 nm.

3.2. Multilayer coatings with different cycles

After the cycle period of the multilayer coatings was optimized, coatings with 24, 48 and 96 cycles were further investigated. Fig. 4 shows one representative cross-section and surface morphology of TiN/Zr/ZrN multilayer coatings. The thickness of total multilayer coatings and each cycle was estimated to be 26.5 μm and 270 nm, respectively. Although the interface is not strictly straight, the thickness for each cycle is nearly constant. By our present auto-control method, we can approximately reproduce our results under the same experimental parameters. This is crucial for multilayer coatings to accomplish industrial applications. For the surface morphology of 96 cycles coatings, the droplet in size of 3~5 μm can be observed, which may be the failure source of erosion test.

Fig. 5 shows the XRD pattern of the deposited multilayer coatings. The diffraction peaks were indexed as cubic TiN and ZrN according to the JCPDS card (No. 02–0956 and No. 38–1420). It can be seen that the diffraction information is dominated by cubic ZrN and TiN phases. The strongest peak corresponds to the (111) plane of ZrN phase with a FCC structure. The hexagonal structure Zr is

Table 1
The basic properties of the multilayer coatings with different cycle periods.

Cycle number	Thickness/μm	Hardness/GPa	Adhesive force/N	Sand weight/g	
				30°	90°
3	7.43	25.83	42	19.0	6.7
12	8.47	29.58	50	21.7	8.1
24	8.50	33.54	70	23.8	8.4

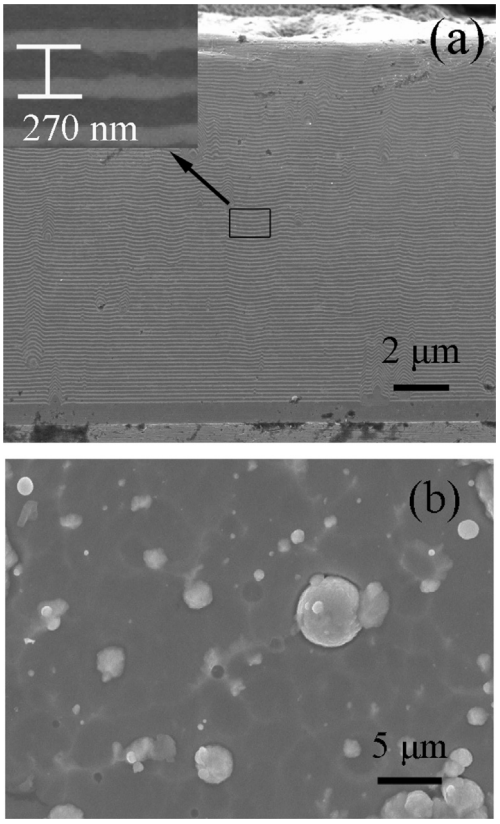

Fig. 4. (a) Representative cross-section and (b) surface of the multilayer sample with 96 cycles.

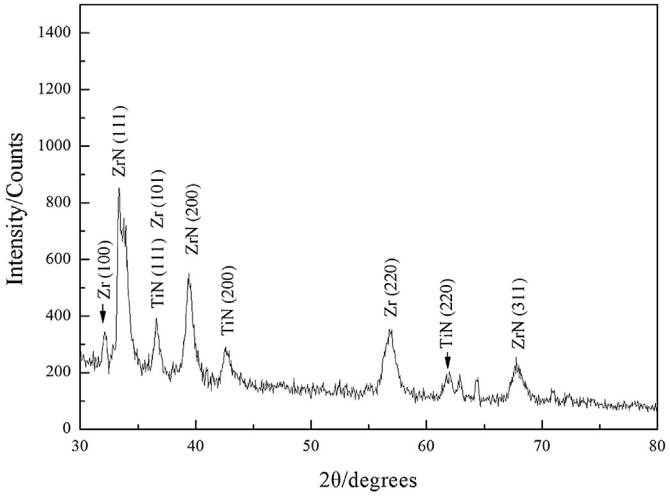

Fig. 5. Representative XRD pattern of the multilayer sample with 96 cycles.

clearly detected whereas no Ti diffraction peak can be observed. However, the Ti layer cannot be excluded since the Ti layer was located at the bottom of the TiN/Zr/ZrN cycle period, its diffraction signal is too weak to be detected.

Fig. 6 shows the AES depth profile of TiN/Zr/ZrN multilayer coatings. The Zr can be clearly observed. The ratio of metal and nitride cannot be discriminated due to the overlapping N KLL and Ti LMM Auger transition peaks. The coating can be divided into two

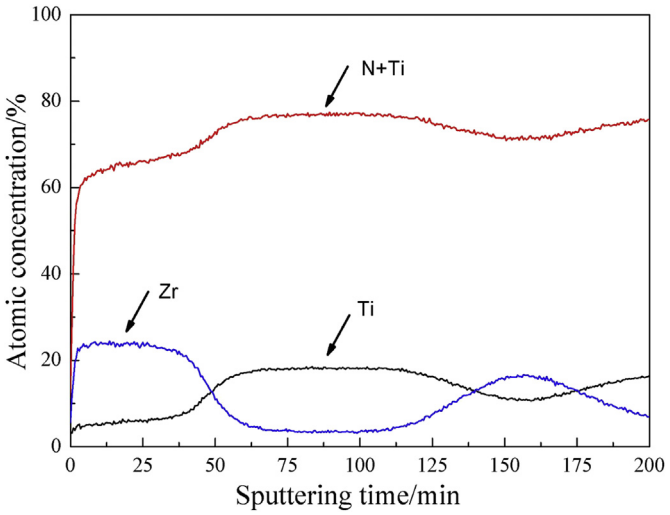

Fig. 6. Depth composition of the multilayer sample with 96 cycles characterized by AES.

repeated TiN and Zr/ZrN with a layer thickness of ~300 nm, consistent with the thickness shown in Fig. 3. The thickness of TiN is thicker than that of Zr/ZrN, which agrees well with our modulated layer.

The effect of the number of cycle (24, 48, and 96 cycles) on Vickers hardness and critical load is shown in Fig. 7. For Vickers hardness, each sample was measured five times. The average value of Vickers hardness for coatings with 24, 48, and 96 cycles is 33.54 GPa (standard error 0.76), 34.25 GPa (standard error 0.54), and 35.42 GPa (standard error 0.76), respectively. As the number of cycle increases from 24 to 96, the hardness value increases slightly from 33.54 GPa to 35.42 GPa. This reveals that the number of cycle does not show much effect on hardness value. With regard to critical loads, they also show a similar trend as hardness. For samples with different cycles, their critical loads are higher than 70 N, which means that all of our coatings have good adhesion to TC_{11} substrates. Overall speaking, variations of the number of cycle do not show obvious effect on hardness and critical load.

Here we mainly focus on two different kinds of multilayer films. The first kind corresponds to the deposited films that they

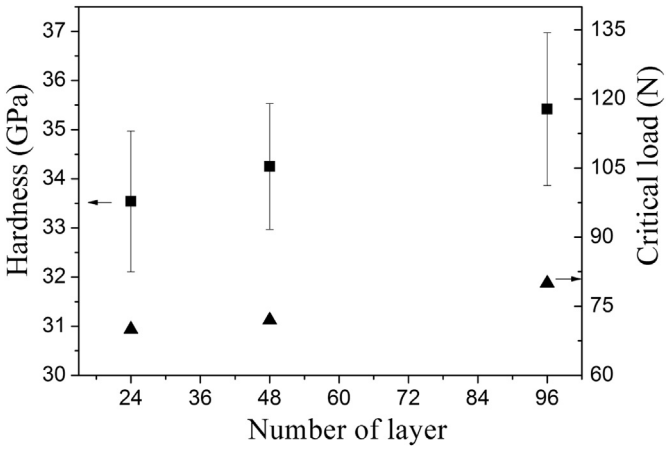

Fig. 7. Hardness and critical load as a function of the number of cycle (error bars, standard deviations).

have a similar film thickness but variable cycle periods. In other words, the film thickness is fixed, but the cycle period is different. The second kind belongs to the prepared films that they have the same optimized cycle period but different film thickness. Namely, they have the same basic unit, but different number of the basic unit. For the first kind of films, the hardness can obviously be tuned as revealed in Table 2. A higher hardness value corresponds to a higher cycle period. This can be explained as follows. A high number of cycle period results in the thickness decrement of the basic cycle unit, which in turn impedes the columnar structure with <111> preferred growth. This leads to a dense structure [22]. A higher cycle period can also increase the number of interface [23]. For the Ti/TiN/Zr/ZrN coatings with 3, 12 and 24 periods, the number of interface is 11, 47 and 95 respectively. The high interface density can block the movement of dislocation, which further improves the hardness of our multilayer films [24]. In addition, we have also checked the effect of the residual stress on the hardness. We find that the residual stress decreases as the number of the cycle period increases. This means that the residual stress and the hardness show two different trends as a function of the number of the cycle period. In general, the increment of the residual stress can improve the hardness of a film [25]. But here in our multilayer films, the residual stress presents an opposite trend. Thus the residual stress may not play the crucial role to affect the hard of multilayer films within our film systems. For the second kind of films, the basic unit is the same. As the number of the basic unit increases, i.e., 24, 48 and 96, the micro-hardness tends to a constant although there are some fluctuations seen from Fig. 7 and Table 3. This is mainly because the hardness measurement gradually eliminates the effect of substrate when the film thickness increases.

3.3. Erosion properties of coatings with variable number of cycle

The erosion test was carried on bare and coated TC_{11} titanium alloys with different number of TiN/Zr/ZrN layer by impact angles of 30° and 90°, respectively. The erosion resistance was estimated by the depth of the erosion pit under the condition of the same amount of erosion sand. Fig. 8 shows the erosion depth as a function of sand amount at 30° impact angle. As expected, coated samples have better erosion resistance comparing with bare substrate. For bare substrate, the erosion rate is nearly constant as sand weight increases, which indicates that the damage of bare substrate starts at the very beginning of the erosion test. But for coated samples, the erosion rate is small at the beginning. After a certain amount of sand weight, the erosion rate is changed into the one that is nearly the same as that of the bare substrate. This indicates that multilayer coatings are pierced. For the damage of coated samples, different number of layer corresponds to different amount of sand erosion. Multilayer coatings start to be damaged with the sand weight of ~22.5 g for coated samples with 24 cycles, ~45 g for 48 cycles, and ~120 g for 96 cycles. For the sample with 96 cycles, the erosion resistance is improved ~5 times. The corresponding depth of the erosion pit is only about 1/10 of that of bare substrates. Even after the coatings are pierced, the erosion depth of the coated samples is still smaller than that of bare substrates. For comparisons, Fig. 9 shows the erosion resistance performance at 90° impact angle. Samples with 24 cycles start to be damaged at the sand amount of 6.0 g, 6.0–9.0 g for the sample with 48 cycles, and 18–24 g for the sample with 96 cycles. Their depths of erosion correspond to 10.8 μm, 12.5 μm, and 22.8 μm, respectively. At the erosion depth

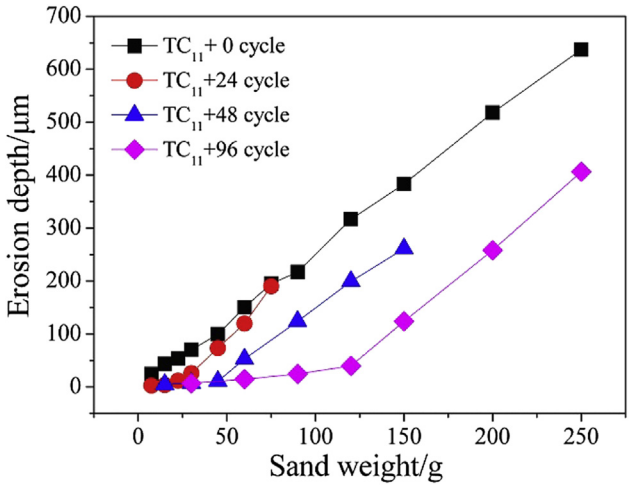

Fig. 8. Erosion resistance as a function of sand weight for bare substrate and multilayers sample with 24, 48, and 96 cycles at the impact angle of 30°.

Table 2
Residual stress and mechanical properties of multilayer films with different cycle periods.

Modulated period	Residual stress/GPa		Adhesive force/N	Hardness/GPa
	Si substrate	TC_{11} substrate		
ZrN	−2.767	−4.165	43	19.37
TiN	−2.392	−4.098	46	18.13
1 cycle	−1.252	−3.526	49	20.61
2 cycle	−0.781	−3.215	54	22.38
4 cycle	−0.565	−3.153	56	24.18
8 cycle	−0.493	−3.081	58	25.48

Table 3
Residual stress and mechanical properties of multilayer films with different thickness.

Film thickness/μm	Residual stress/GPa		Adhesive force/N	Hardness/GPa
	Si substrate	TC_{11} substrate		
2.32	−0.493	−3.081	58	25.48
4.31	−0.629	−2.991	62	27.47
7.54	−0.810	−3.091	66	30.66
9.29	−1.216	−3.136	71	30.91

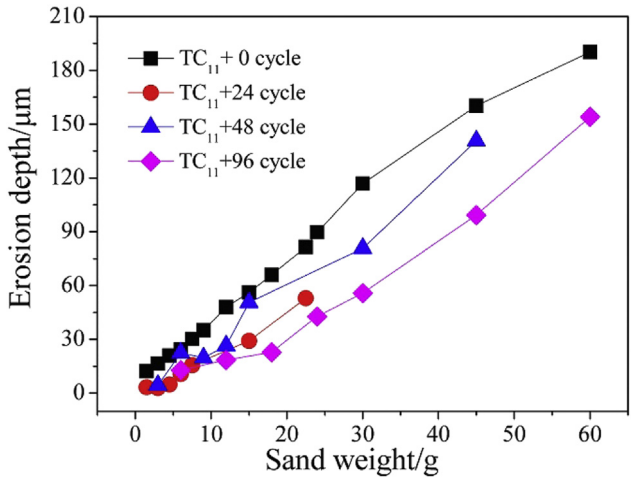

Fig. 9. Erosion resistance as a function of sand weight for bare substrate and multilayers sample with 24, 48, and 96 cycles at the impact angle of 90°.

of 22.8 μm for coatings with 96 cycles, the erosion depth for bare substrates has already reached up to 66 μm. The depth of erosion in coated sample is only about 1/5–1/3 of that of the bare samples.

For the erosion behavior at impact angles of 30° and 90°, some features can be described as follows. The coating surface starts to damage in stress concentration areas or pits where droplets fall as shown in Fig. 4. As the sand amount increases, the erosion depth is slightly changed firstly, and then increased sharply. The erosion depth of coated samples is always smaller than that of substrate materials under the same sand amounts. In general, the sand erosion properties can be improved by TiN/Zr/ZrN multilayer coatings.

Here the failure mechanism is also discussed. Fig. 10a shows the eroded surface morphology of bare TC_{11} titanium samples at 30° impact angle. When impacting particles strike the surface of titanium alloys, the movement of impacting particles is decomposed into horizontal and normal ones [26]. The horizontal movement of impacting particles plays a leading role in dominating material loss through cutting or plowing material surfaces. The process is mainly related to plastic deformation. Therefore, shear zones can be clearly observed on the eroded surface in Fig. 10a. This is a common feature of material removal for ductile metals under the condition of sand particle erosion [27].

For the erosion at 90° impact angle (Fig. 10b), erodent particles strike the surface of TC_{11} titanium samples from the vertical direction. The horizontal movement of erodent particles is neglected. Correspondingly, shear zones are not easily observed. In contrast, irregular pits (or indentations) can be easily observed on material surfaces. This is probably due to the removal of a surface chip on the edge of indentations caused by impacting particles [26].

For coated samples, Fig. 11a shows the morphology of eroded surface at 30° impact angle. The area marked as “A” in Fig. 11a seems to be layered flaking. This can be seen clearly from the edge of the enlarged zone (Fig. 11b). In general, damages caused by sharp erodent particles are associated with plastic cutting or radial cracking in brittle materials [27]. However, neither plastic cutting nor radial cracking can be clearly observed in the crater as marked “B” in Fig. 11a and c.

For coated samples at 90° impact angle, Fig. 12a shows the exfoliation of coatings in the marked B area, which can be seen clearly from the edge of the crater in the enlarged zone (Fig. 12c). Under this circumstance, the mechanism of material removal can

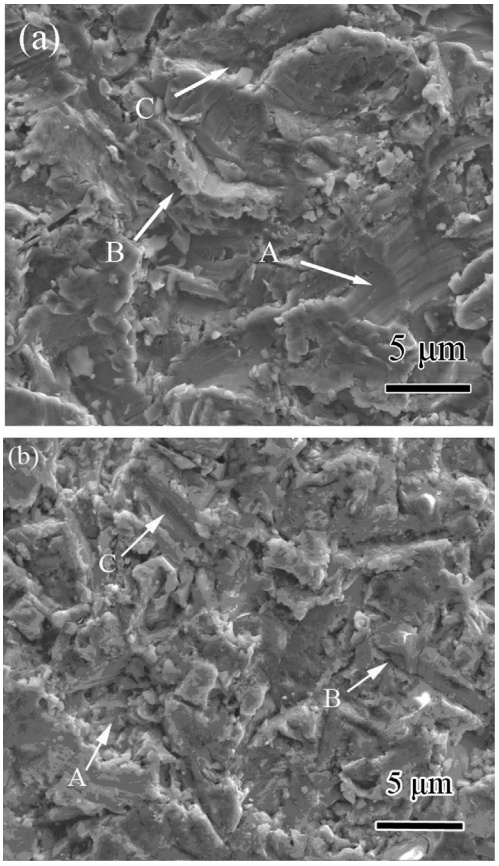

Fig. 10. Eroded surface morphology of the bare substrate. (a) eroded at the impact angle of 30°. (b) eroded at the impact angle of 90°.

be understood as follows. Material surfaces are continuously impacted by angular erodent particles. Micro-cracks may be generated and extended laterally underneath the surface of samples. Once these cracks connect with each other during the process of successive erosion, materials in some localized area will be delaminated. This can be seen clearly from the irregular delamination on the edge of the crater in Fig. 12c. Our results here agree with previous observations [28,29]. In addition, we further examined the eroded morphology of the multilayer samples with 96 cycles at 90° impact angle. As shown in Fig. 13, cracks can be deflected (zone C) and branched (zones A and B) when they propagate in multilayer coatings. For comparison, typical cracks in TiN/NbN multilayer coating from previous work show not obvious deflection [15]. Crack deflection can change the propagation direction of cracks. Branched cracks can weaken intensive stress distributions ahead of crack tip. Our new architectures have better resistance against crack extension. Therefore, sand erosion properties of substrates are improved.

4. Conclusions

A new architecture, TiN/Zr/ZrN multilayer with different period and number of cycle were deposited on TC_{11} titanium substrates by multi-target vacuum cathodic arc ion plating method. Under the condition of similar film thickness, samples with 24 periods have higher hardness and critical load than those with 3 and 12 periods, indicating better erosion resistance properties can be obtained. For coatings with variable cycles, the

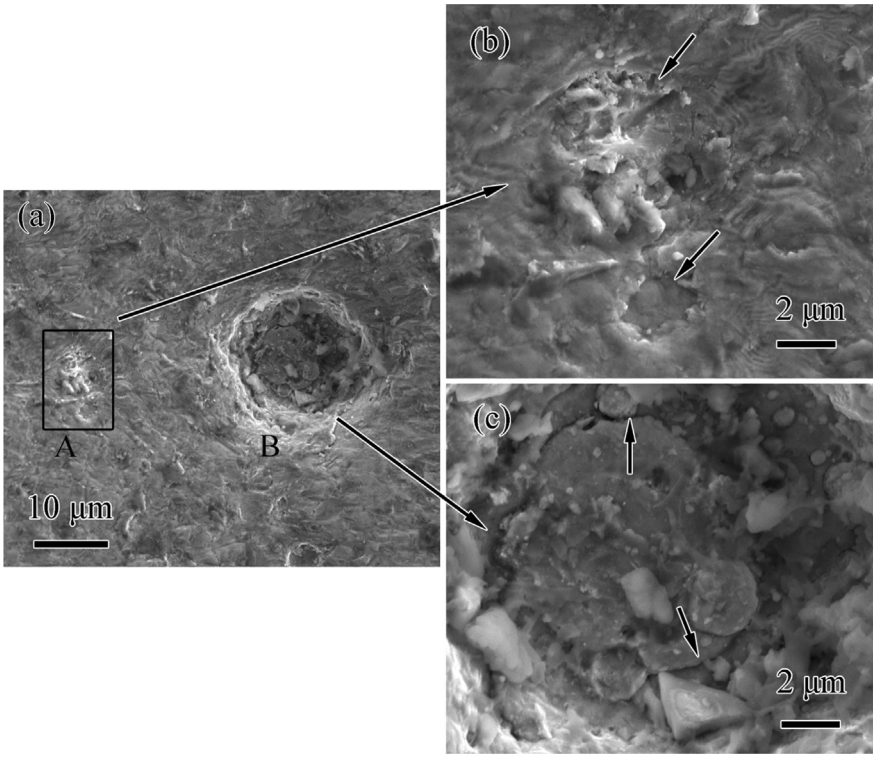

Fig. 11. Eroded surface morphology of the coated sample with 96 cycles eroded at the impact angle of 30°.

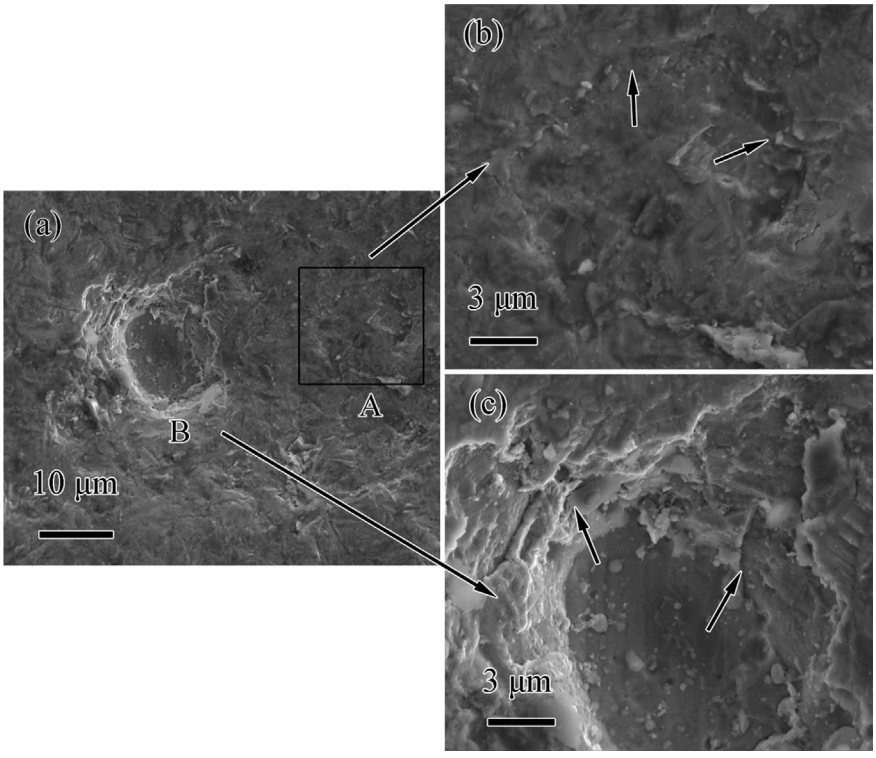

Fig. 12. Eroded surface morphology of the coated sample with 96 cycles eroded at the impact angle of 90°.

hardness values have no obvious changes, from 33.54 GPa for the sample with 24 cycles to 35.42 GPa for the one with 96 cycles. The failure mechanism is different for bare substrate and coated samples. For bare substrate, cutting and plowing dominate material failure, exhibiting the ductile feature. While for coated samples, the mechanism of material removal may be due to the

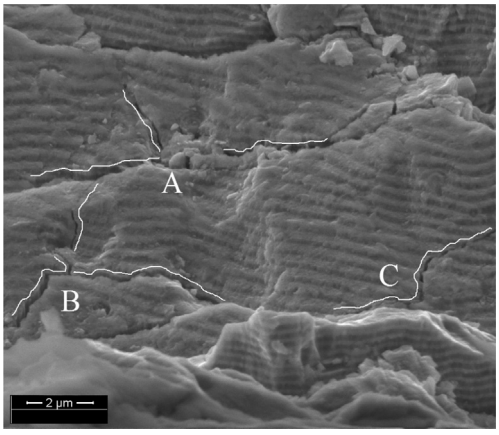

Fig. 13. Crack deflection and crack branching of the multilayers sample with 96 cycles at the impact angle of 90°.

lateral extension and succeeding interaction of micro-cracks, presenting the brittle feature.

Acknowledgment

This work was supported by Guangdong International Cooperation Project under project number of 2011B050400007.

References

[1] Y. Sahin, O. Durak, Mater Des. 2007 (1844) 28.
[2] Y.Y. Santana, J.G. La Barbera-Sosa, A. Bencomo, J. Lesage, D. Chicot, E. Bemporad, et al., Surf. Eng. 28 (2012) 237.
[3] J.L. Cao, K.L. Choy, H.L. Sun, H.Q. Li, D. Teer, M.D. Bao, J. Coat. Technol. Res. 8 (2010) 283.
[4] K. Bose, R.J.K. Wbod, Wear 258 (2005) 366.
[5] P. Yan, J.X. Deng, Z. Wu, S.P. Li, Y.Q. Xing, J. Zhao, Int. J. Refract Met. Hard Mater 35 (2012) 213.
[6] A. Feuerstein, A. Kleyman, Surf. Coat. Technol. 204 (2009) 1092.
[7] D.W. Wheeler, R.J.K. Wood, Wear 250 (2001) 795.
[8] L. Guo, G. Chen, Diam. Relat. Mater 16 (2007) 1530.
[9] C.K. Lee, Appl. Surf. Sci. 254 (2008) 4111.
[10] T. Grogler, E. Zeiler, M. Dannenfeldt, S.M. Rosiwal, R.F. Singer, Diam. Relat. Mater 6 (1997) 1658.
[11] J.X. Deng, F.F. Wu, Y.S. Lian, Y.Q. Xin, S.P. Li, Int. J. Refract Met. Hard Mater 35 (2012) 10.
[12] Y.S. Li, C.Z. Zhang, H.T. Ma, L.Z. Yang, L.L. Zhang, Y. Tang, et al., Mater Chem. Phys. 134 (2012) 145.
[13] R. Ikeda, M. Hayashi, A. Yonezu, T. Ogawa, M. Takemoto, Diam. Relat. Mater 13 (2004) 2024.
[14] U. Wiklund, P. Hedenqvist, S. Hogmark, Surf. Coat. Technol. 97 (1997) 773.
[15] B. Borawski, J.A. Todd, J. Singh, D.E. Wolfe, Wear 271 (2011) 2890.
[16] B. Borawski, J. Singh, J.A. Todd, D.E. Wolfe, Wear 271 (2011) 2782.
[17] Q. Yang, D.Y. Seo, L.R. Zhao, Surf. Coat. Technol. 177–178 (2004) 204.
[18] K.L. Rutherford, I.M. Hutchings, Surf. Coat. Technol. 86–87 (1996) 542.
[19] J.S. Koehler, Phys. Rev. B 2 (1970) 547.
[20] D.W. Celotta, U.A. Qureshi, E.V. Stepanov, D.P. Goulet, J. Hunter, C.H. Buckberry, et al., Wear 263 (2007) 278.
[21] Y. Purandare, M.M. Stack, P. Hovsepian, Wear 259 (2005) 256.
[22] J.C. Caicedoa, C. Amaya, L. Yatec, O. Nosc, M.E. Gomeza, P. Prieto, et al., Mater. Sci. Eng. B 171 (2010) 56.
[23] S.J. Bull, A.M. Jones, Surf. Coatings Technol. 78 (1996) 173.
[24] P.C. Yashar, W.D. Sproul, Vacuum 55 (1999) 179.
[25] C.L. Chang, J.Y. Jao, W.Y. Ho, D.Y. Wang, et al., Vacuum 81 (2007) 604.
[26] G.P. Tilly, Wear 23 (1973) 87.
[27] P.H. Shipway, I.M. Hutchings, Wear 193 (1996) 105.
[28] X.J. Wang, M.H. Fang, L.C. Zhang, H. Ding, Y.G. Liu, Z.H. Huang, et al., Mater Chem. Phys. 139 (2013) 765.
[29] E. Bousser, L. Martinu, J.E.K. Sapieha, Surf. Coat. Technol. 235 (2013) 383.